Tunable acoustophoretic band-pass particle sorter

Jonathan D. Adams[1] and H. Tom Soh[2,a)]
[1]*Department of Physics, University of California, Santa Barbara, California 93106, USA*
[2]*Department of Mechanical Engineering and Department of Materials, University of California, Santa Barbara, California 93106, USA*

(Received 23 May 2010; accepted 25 June 2010; published online 13 August 2010)

Acoustophoretic separation in microchannels offers a promising avenue for high-throughput, label-free, cell and particle separation for many applications. However, previous acoustophoretic separation approaches have been limited to a single size separation threshold, analogous to a binary filter, (i.e., high-pass or low-pass). Here, we describe a tunable acoustophoretic separation architecture capable of sorting cells and particles based on a range of sizes, analogous to a band-pass filter. The device is capable of sorting an arbitrary range of particle sizes between 3 and 10 μm in diameter with high efficiency (transfer fraction$=0.98\pm0.02$) at a throughput of $\sim 10^8$ particles/h/microchannel. © *2010 American Institute of Physics*. [doi:10.1063/1.3467259]

For many biotechnological applications where specific surface markers are not available, separation methods based on physical properties offers an important avenue for enriching target populations of cells and particles from complex mixtures. For example, live and dead cells have been sorted based on their different polarization responses,[1–3] and mammalian cells have been purified according to their phase in the cell cycle based on volume.[4–7] Other physical parameters such as density, magnetic susceptibility, and refractive index have been utilized for cell sorting by means of dielectric, magnetic, mechanical, hydrodynamic, or optical forces.[8,9]

In particular, acoustophoretic separation in microfluidic channels has received significant recent interest because the technique does not depend on buffer conductivity or *p*H and offers gentle, high throughput separation based on size, density, and compressibility.[10] Recently, many applications of acoustic separation in microchannels have emerged, including label free separation of lipids,[11,12] mammalian cells,[6,13] and blood.[14] To date, however, microfluidic acoustic separation techniques have only allowed separations based on a single size threshold, analogous to high-pass or low-pass filters, and were incapable of purifying target species based on a range of sizes (i.e., band-bass). For many applications, the capability to tune both an upper and lower size threshold in a single device would enable additional functionality. Toward this goal, we report the acoustic band-pass particle sorter (ABPS)—a microfluidic acoustic separation device with fully adjustable size-based separation. We show high efficiency separation (transfer fraction$=0.98\pm0.02$) with fully tunable upper and lower size threshold in the range of $3-10$ μm in diameter, at a high throughput ($\sim 10^8$ particles/h/microchannel).

The ABPS is a three-input, three-output device and consists of two serially integrated separation stages (Fig. 1). The mechanism of acoustic separation has been described in the pioneering work of Laurell and co-workers as well as our group.[6,10,11,14,15] Briefly, piezoelectric transducers attached to the device generate a resonant pressure field within the fluidic channel of the device with a pressure node along the half-width of the channel, resulting in a transverse force $F_{ac,t}$ given by

$$F_{ac,t}=\frac{8\pi^2 E r^3 f}{3c_o}\left[\frac{5\alpha-2}{2\alpha+1}-\frac{1}{\alpha\beta^2}\right]\sin\frac{4\pi f y}{c_o} \quad (1)$$

for spherical particles, where E is the acoustic energy density, r the particle radius, f is the actuation frequency, y the transverse position in the channel, and $\alpha=\rho_p/\rho_o$ and $\beta=c_p/c_o$, with $\rho_{p(o)}$ the particle (medium) density and $c_{p(o)}$ the speed of sound in the particle (medium). Since inertial effects are negligible at the low Reynolds number ($Re_{ABPS}\sim 15$) in our system, the transverse acoustic force is

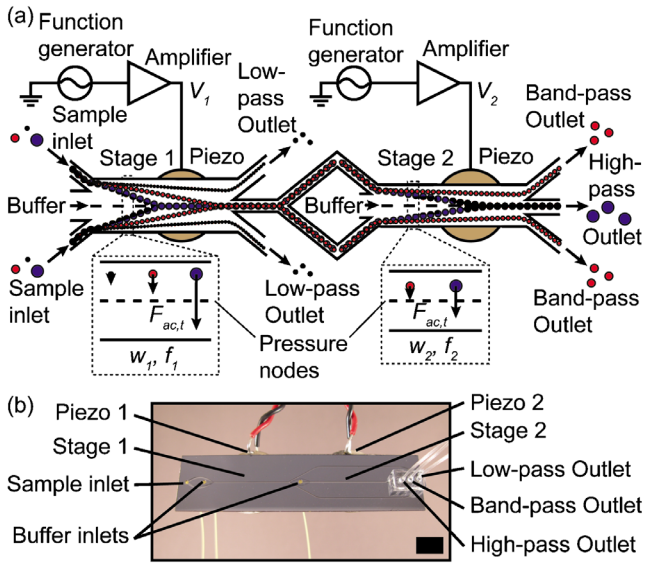

FIG. 1. (Color online) (a) The ABPS consists of two independently controlled, serially connected stages, each characterized by a channel width w, and piezo actuation amplitude V and frequency f. A particle mixture of varied sizes is introduced into the sides of stage 1 alongside a central buffer flow. Due to the volume dependence of the acoustic radiation force, larger particles are focused faster than smaller particles. The larger, selected particles are reintroduced into the sides of stage 2 and subject to another round of independently controlled focusing. By selecting appropriate operating parameters (flow rate, V and f), any range of particle sizes particle can be sorted into the band-pass outlet. (b) Photograph of the ABPS. The scale bar corresponds to 1 cm.

a)Author to whom correspondence should be addressed. Electronic mail: tsoh@engineering.ucsb.edu.

counterbalanced by Stokes' drag acting on the particle, resulting in an equation of motion given by $F_{ac,i}=6\pi\eta r dy/dt$, where η is the fluid viscosity. Additionally, since $E\propto V^2$,[16] where V is the amplitude of the voltage applied to the transducer, the transverse focusing speed of particles $dy/dt\propto V^2r^2$. Thus, particles of different size focus at different rates, and the overall focusing may be scaled by adjusting the actuation voltage of the piezotransducer.

The different channel widths w_1 and w_2 of the two stages allow each transducer to be actuated at two distinct resonant frequencies f_1 and f_2 and applied voltages V_1 and V_2, leading to independent control over the pressure field in each stage of the ABPS.[15,17] The sample, consisting of a mixture of particles, is introduced into the sides of stage 1 along with a central buffer flow [Fig. 1(a), left]. The volume-dependent acoustic radiation force focuses the larger particles to the center of the channel, transferring them to stage 2 of the device. The unselected, smaller particles are eluted into the low-pass outlet. Stage 2 uses the same selection mechanism, at different amplitude, to further elute the largest particles to the high-pass outlet, while directing the target particles to the band-pass outlet [Fig. 1(a), right]. A photograph of the ABPS device is shown in Fig. 1(b). The channel widths w_1 and w_2 are 350 μm and 400 μm, respectively. All other channel widths were calculated such that the central $\sim 1/7$ of the total flow from stage 1 was transferred into stage 2, and their values range between 52 and 271 μm. A fabrication protocol and experimental setup detail are provided in the supplemental information.[18]

The separation performance of the ABPS was measured using a sample mixture of 10-, 5-, and 3-μm-diameter fluorescent polystyrene particles (G1000, G0500, R0300, Microgenics Corp., Fremont, CA), suspended at a concentration of $\sim 10^7$ particles/ml (calculated based on stock bead solutions of 1% w/v solids) in a buffer solution of ultrapure water with 0.01% v/v Tween-20 (Sigma-Aldrich, St. Louis, MO). The sample and buffer inputs were pumped at flow rates of 2 ml/h and 14 ml/h, respectively. The applied peak-to-peak voltages were varied between 0 and 43 V which was the limit of our amplifier. The operational frequency for each stage was chosen by monitoring the focusing response and were $f_1=2.105$ MHz and $f_2=1.892$ MHz (see supplemental information[18]). For each piezotransducer voltage setting, the device was run for 5 min before collecting samples from each of the device outlets, to ensure that all fluid from the previous setting was flushed from the outlet tubing. Collected samples were subsequently analyzed via flow cytometry (FACSAria, BD Biosciences, San Jose, CA). To quantify the separation performance, we define the transfer fraction Γ_i, which is the fraction of particles of size i transferred into the band-pass outlet, as

$$\Gamma_i = \frac{\gamma_B N_{b,i}}{\gamma_B N_{B,i} + \gamma_L N_{L,i} + N_{H,i}}, \tag{2}$$

where γ is the outlet flow rate relative to the high-pass outlet and N is the counts from cytometry analysis for particle i, with subscripts L, B, and H referring to the low-pass outlet, band-pass outlet, and high-pass outlet, respectively.

In order to characterize each stage independently, we initially increased V_1 while leaving the second piezotransducer unactuated. As shown in Fig. 2(a), we observed controllable transfer of particles into the band-pass outlet. The

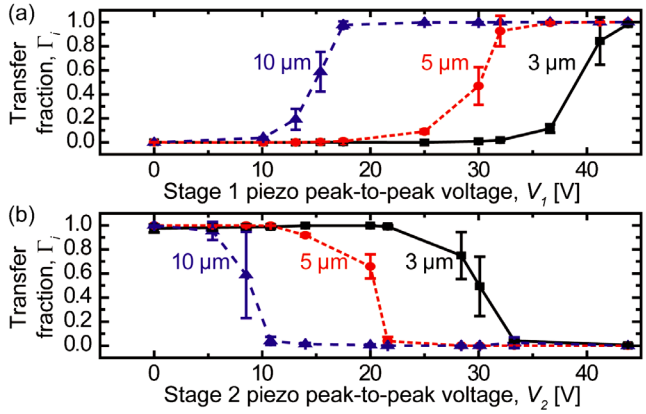

FIG. 2. (Color online) Transfer fraction of particles as a function of applied voltage for each separation stage. (a) The stage 1 piezo was driven with a sinusoidal signal (V_1) at 2.105 MHz, while the stage 2 piezo was not actuated. As V_1 is increased, successively smaller particles are transferred into stage 2 and eluted through the band-pass outlet. (b) The stage 1 piezo was driven at 2.105 MHz and 43 V peak-to-peak, while the stage 2 piezo was driven at 1.892 MHz and swept in driving amplitude. Thus, all particles were initially directed into the band-pass outlet and as the driving voltage for stage 2 was increased, particles were selectively transferred out of the band-pass outlet into the high-pass outlet. In both (a) and (b), the data points show mean and standard deviations over three independent experiments.

threshold peak-to-peak voltages for particle transfer, defined as $\Gamma_i=0.5$, were 15.0 ± 0.6 V (10 μm), 30.0 ± 0.9 V (5 μm), and 39.2 ± 0.9 V (3 μm). At maximum actuation voltage of 43 V, we measured $\Gamma_{3\ \mu m}=0.98\pm0.02$, $\Gamma_{5\ \mu m}=1$, and $\Gamma_{10\ \mu m}=1$, indicating near-ideal transfer into the band-pass outlet. We next maintained V_1 at maximum amplitude and scanned V_2 [Fig. 2(b)]. We observed a similar response wherein the larger particles focused into the high-pass outlet more easily than smaller particles. With both transducers actuated at maximum amplitude, we measured $\Gamma_{3\ \mu m}=0.005\pm0.009$, $\Gamma_{5\ \mu m}=0$, and $\Gamma_{10\ \mu m}=0$, again indicating near-ideal transfer into the high-pass outlet. In theory, the relationship between the particle radius and the voltage necessary for focusing should be that $V\propto 1/r$; this appears to hold true for both stages [supplemental Fig. 1 (Ref. 18)]. We observed lower threshold peak-to-peak voltages required for focusing in stage 2 (9 ± 1 V, 19 ± 2 V, and 30 ± 1 V for the 10 μm, 5 μm, and 3 μm particles, respectively). This is likely due to a minimal coupling of energy that occurred between the two stages [see supplemental Fig. 2 (Ref. 18)].

Next, we show that, by tuning V_1 and V_2, any combination of 10-, 5-, and 3-μm-diameter particles can be directed to elute through the band-pass outlet. Here, we prepared a mixture of 10, 5, 3, and 1 μm diameter fluorescent polystyrene particles (G1000, G0500, R0300, B0100, Microgenics Corp., Fremont, CA) and suspended it at a concentration of $\sim 10^8$ particles/ml in buffer solution, calculated based on stock bead solutions of 1% w/v solids. After setting the flow rates of the sample (2 ml/h) and buffer (14 ml/h), we adjusted V_1 and V_2 such that defined particle populations were completely transferred into the band-pass outlet, while undesired particles were eluted to either the low-pass outlet or the high-pass outlet. Adjustment of V_1 controlled the lower size threshold, while V_2 controlled the upper size threshold. The six possible combinations of the 3, 5, and 10 μm particles were investigated; Fig. 3 shows that we were able to direct any continuous combination of 3, 5, and 10 μm particles into the band-pass outlet with high efficiency. The driv-

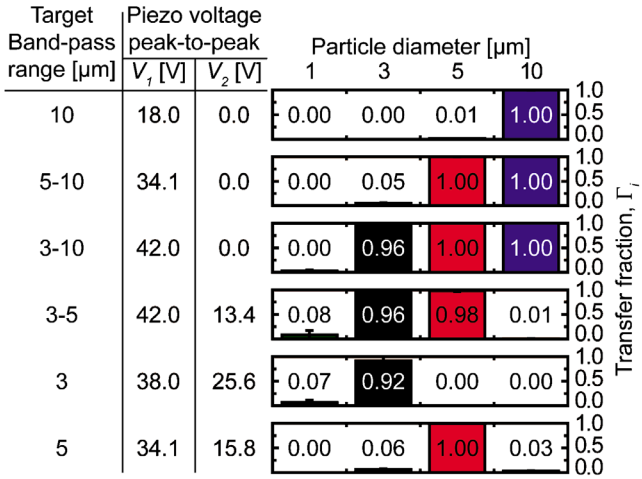

FIG. 3. (Color online) Transfer fraction into the band-pass outlet as a function of particle size. V_1 and V_2 can be configured such that any combination of 10, 5, and 3 μm particles will elute through the band-pass outlet. From left to right, each column in the figure shows the target range of particle sizes in the band-pass outlet, the corresponding actuation peak-to-peak voltages of each piezotransducer and the transfer fraction for each particle size at that setting over three independent experiments. From all separation data, the average transfer fraction for target particles intended for the band-pass outlet was 0.98 ± 0.04, and 0.02 ± 0.04 for nontarget particles.

ing voltages required for each are listed in the middle columns in Fig. 3 and corresponded well with the results from Fig. 2(a). The average Γ_i for any particle selected in the band-pass outlet was 0.98 ± 0.4 and 0.02 ± 0.04 for any particle excluded from the band-pass outlet. The purity of the band-pass outlet fractions, or ratio of the total desired to the total number of particles in the band-pass outlet, ranged from 0.4 ± 0.2 to 0.93 ± 0.03. This performance in throughput and purity compare favorably with previously reported microfluidic approaches.[8]

We believe the ultimate resolution of the ABPS to separate particles that are similar in dimension will be governed by not only by the accuracy of applying the acoustic separation force, but also by flow profile in the microchannel coupled with variations in the particle starting positions. Due to the sample inlet channels having widths of 50 μm, particles will initially be transported along the channel at different rates and start at different distances from the pressure node. Prefocusing the particles to a more uniform starting position may help mitigate this limitation.[19] In addition to the acoustic radiation force, induced steady fluid motion known as acoustic streaming was observed in the microchannel. In comparison with the volume-dependent radiation force, the streaming flow transports particles via Stokes' drag, proportional to the radius. This effect was most notable at the highest driving voltages, where some of the 1 μm particles were observed to be transported along flow rolls characteristic of acoustic streaming. We suspect that acoustic streaming is responsible for the small amount of transfer of 1 μm particles into the band-pass outlet, and that, ultimately, the ability to separate particles less than 1 μm in size may be limited by the phenomenon.

In summary, we have developed a device architecture for acoustic separation that allows for a tunable upper and lower particle size threshold. This was achieved through serial integration of two acoustic separation stages of different width, allowing each stage to be operated independently. We were able to direct any continuous particle size range between 3 and 10 μm in diameter into a single outlet at an estimated throughput of $\sim 10^8$ particles/h, a rate comparable to high-speed flow cytometry.[20] The size range of separable particles matches closely with typical cell sizes and could be potentially extended through better understanding and control of acoustic streaming effects.[21] Given that acoustic separation has been shown to be gentle and does not affect cell viability,[6,22] we envision that our architecture may be a basis for an adaptable and versatile cell sorting system.

We are grateful for the financial support of the ARO Institute for Collaborative Biotechnologies, Office of Naval Research, and National Institutes of Health. We thank Hans C. Meyer and Henrik Bruus for helpful discussions.

[1] A. Docoslis, N. Kalogerakis, L. A. Behie, and K. V. I. S. Kaler, Biotechnol. Bioeng. **54**, 239 (1997).
[2] M. D. Vahey and J. Voldman, Anal. Chem. **80**, 3135 (2008).
[3] H. Shafiee, M. B. Sano, E. A. Henslee, J. L. Caldwell, and R. V. Davalos, Lab Chip **10**, 438 (2010).
[4] P. K. Davis, A. Ho, and S. F. Dowdy, BioTechniques **30**, 1322 (2001).
[5] U. Kim, C.-W. Shu, K. Y. Dane, P. S. Daugherty, J. Y. J. Wang, and H. T. Soh, Proc. Natl. Acad. Sci. U.S.A. **104**, 20708 (2007).
[6] P. Thévoz, J. D. Adams, H. Shea, H. Bruus, and H. T. Soh, Anal. Chem. **82**, 3094 (2010).
[7] S. Choi, S. Song, C. Choi, and J.-K. Park, Anal. Chem. **81**, 1964 (2009).
[8] D. R. Gossett, W. M. Weaver, A. J. Mach, S. C. Hur, H. T. K. Tse, W. Lee, H. Amini, and D. Di Carlo, Anal. Bioanal. Chem. (to be published).
[9] A. Lenshof and T. Laurell, Chem. Soc. Rev. **39**, 1203 (2010).
[10] T. Laurell, F. Petersson, and A. Nilsson, Chem. Soc. Rev. **36**, 492 (2007).
[11] F. Petersson, A. Nilsson, C. Holm, H. Jönsson, and T. Laurell, Lab Chip **5**, 20 (2005).
[12] C. Grenvall, P. Augustsson, J. R. Folkenberg, and T. Laurell, Anal. Chem. **81**, 6195 (2009).
[13] J. V. Norris, M. Evander, K. M. Horsman-Hall, J. Nilsson, T. Laurell, and J. P. Landers, Anal. Chem. **81**, 6089 (2009).
[14] F. Petersson, L. Åberg, A.-M. Swärd-Nilsson, and T. Laurell, Anal. Chem. **79**, 5117 (2007).
[15] J. D. Adams, P. Thévoz, H. Bruus, and H. T. Soh, Appl. Phys. Lett. **95**, 254103 (2009).
[16] R. Barnkob, P. Augustsson, T. Laurell, and H. Bruus, Lab Chip **10**, 563 (2010).
[17] O. Manneberg, S. M. Hagsäter, J. Svennebring, H. M. Hertz, J. P. Kutter, H. Bruus, and M. Wiklund, Ultrasonics **49**, 112 (2009).
[18] See supplementary material at http://dx.doi.org/10.1063/1.3467259 for a description of device fabrication process and experimental setup, analysis of threshold focusing voltage, frequency response measurement, and video of device in operation.
[19] C. Grenvall, P. Augustsson, and T. Laurell, Proceedings of the 13th International Conference on Miniaturized Systems for Chemistry and Life Sciences, Jeju, Korea, (Chemical and Biological Microsystems Society, San Diego,2009), p. 776.
[20] S. F. Ibrahim and G. van den Engh, Curr. Opin. Biotechnol. **14**, 5 (2003).
[21] S. M. Hagsäter, A. Lenshof, P. Skafte-Pedersen, J. P. Kutter, T. Laurell, and H. Bruus, Lab Chip **8**, 1178 (2008).
[22] J. Hultström, O. Manneberg, K. Dopf, H. M. Hertz, H. Brismar, and M. Wiklund, Ultrasound Med. Biol. **33**, 145 (2007).